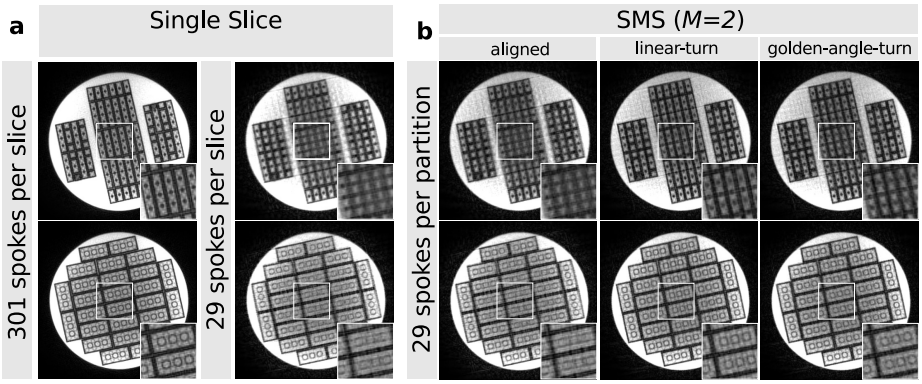

Supporting Figure S1: Comparison of different acquisition and reconstruction strategies for radial measurements on the brick phantom with $N_{\mathrm{sp}} = 29$ spokes per partition or slice and a fully sampled reference scan with $N_{\mathrm{sp}} = 301$ spokes per slice. a) Single-slice acquisition and NLINV reconstruction for each slice. b) SMS acquisition and SMS-NLINV reconstruction for $M = 2$ and aligned (left), linear-turn-based (center) and golden-angle-turn-based sampling (right). Slice distance $d = 60\,\mathrm{mm}$. A magnified region-of-interest indicated by a white rectangle is shown as inset on the bottom right of every image.

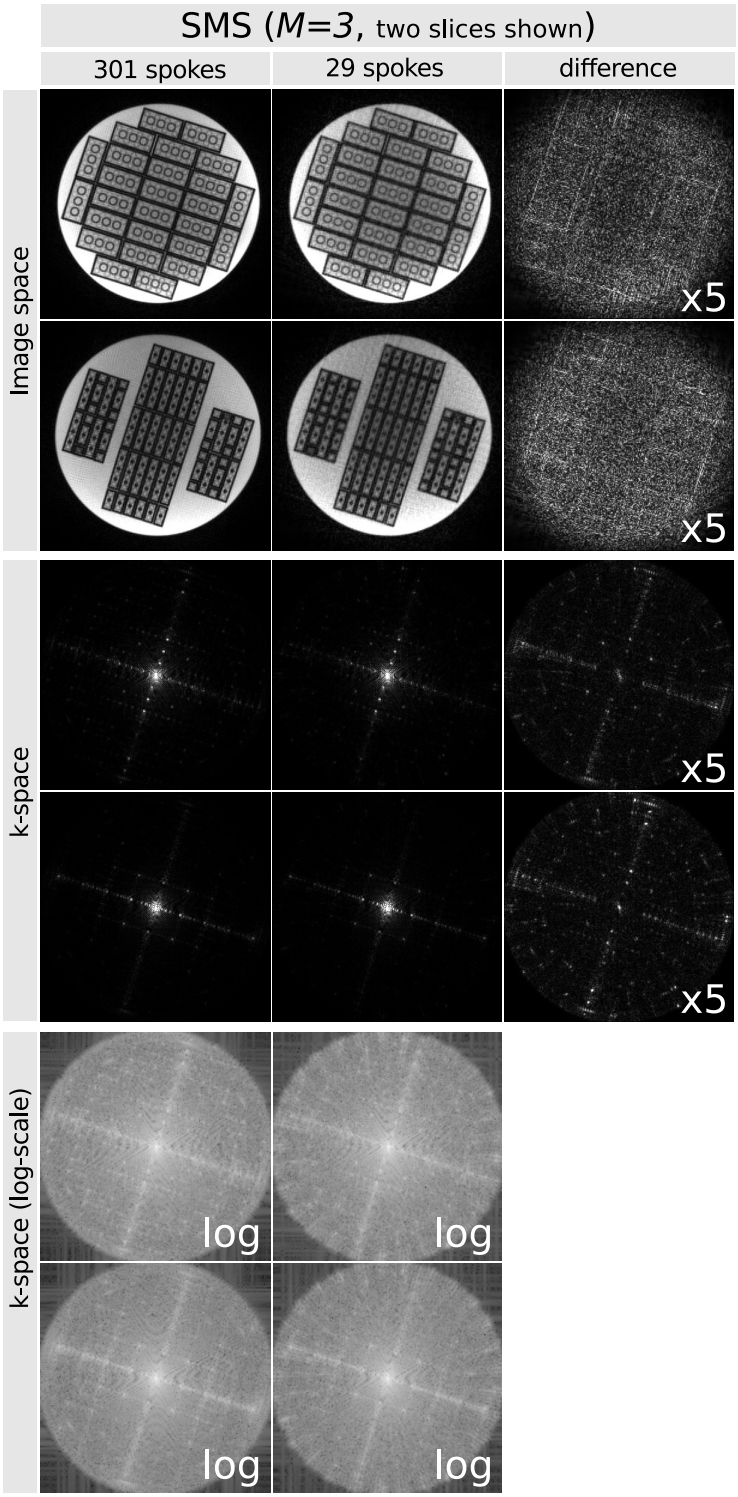

Supporting Figure S2: Difference images in image and k-space for SMS ($M = 3$, slice distance $d = 30\,\text{mm}$, linear-turn-based spoke distribution) acquisitions with $N_{\text{sp}} = 301$ (fully sampled reference) and $N_{\text{sp}} = 29$ spokes per partition. For better visibility, the intensity of the difference images was increased by a factor of 5 and the k-spaces were additionally depicted using the log-scale.

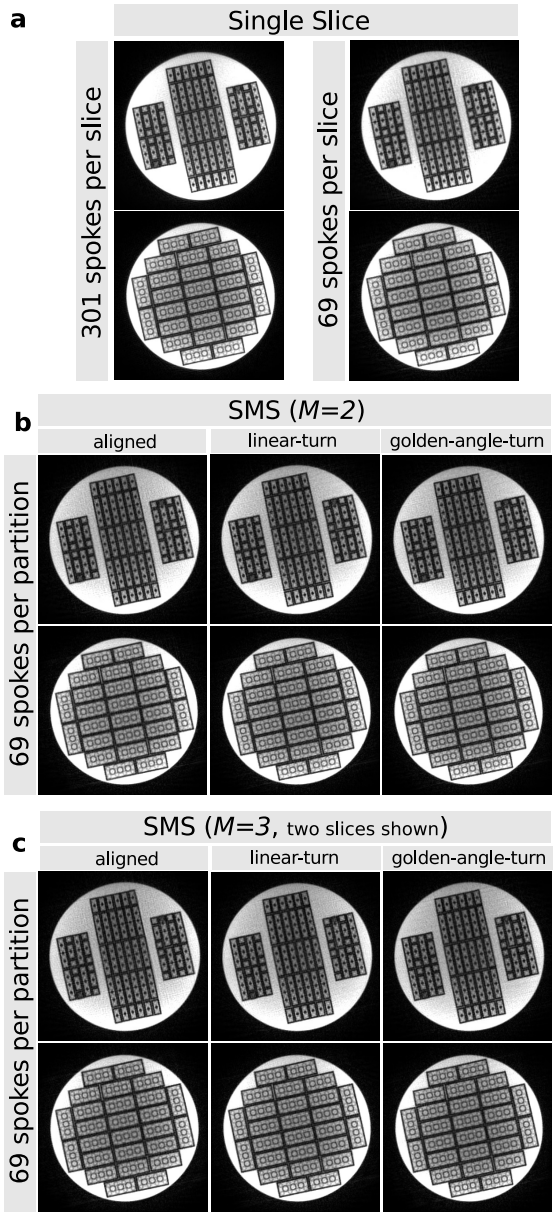

Supporting Figure S3: Comparison of different acquisition and reconstruction strategies for radial measurements on the brick phantom with $N_{\mathrm{sp}} = 69$ spokes per partition or slice and a fully sampled reference scan with $N_{\mathrm{sp}} = 301$ spokes per slice. a) Single-slice acquisition and NLINV reconstruction for each slice. b) SMS acquisition and SMS-NLINV reconstruction for $M = 2$ and aligned (left), linear-turn-based (center) and golden-angle-turn-based sampling (right). Slice distance $d = 60\,\mathrm{mm}$. c) SMS acquisition and SMS-NLINV reconstruction for $M = 3$ and aligned (left), linear-turn-based (center) and golden-angle-turn-based sampling (right). Only the outermost slices with slice distance $d = 60\,\mathrm{mm}$ are depicted.

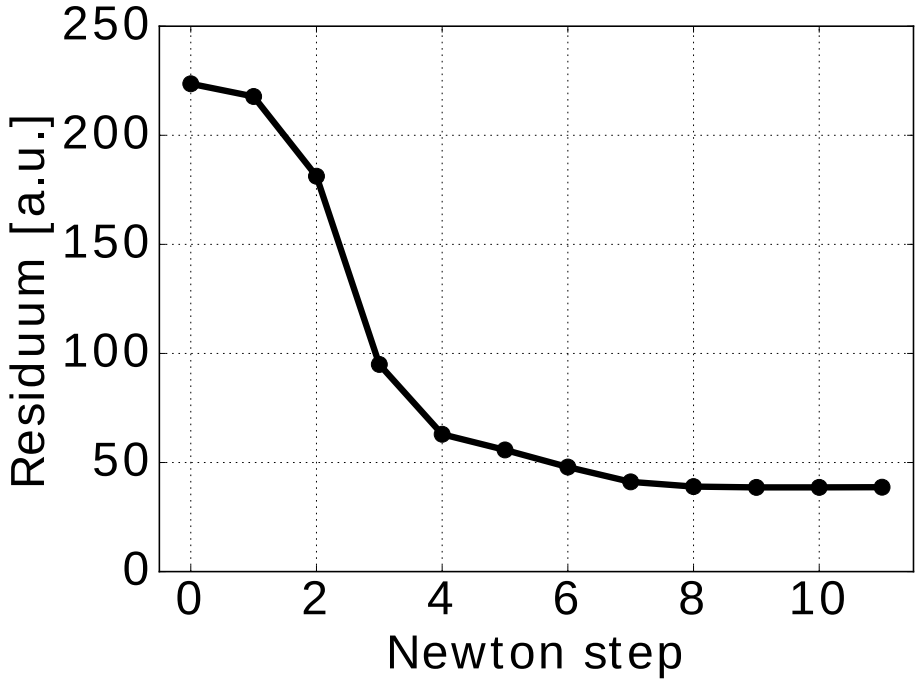

Supporting Figure S4: Residuum of the SMS-NLINV reconstruction in Figure 7 against the number of Newton steps.